Available online at www.sciencedirect.com
ScienceDirect
Progress in Natural Science 18 (2008) 1083–1088
Progress in Natural Science
www.elsevier.com/locate/pnsc

Non-invasive measurement and validation of tissue oxygen saturation covered with overlying tissues

Yichao Teng [a], Haishu Ding [a,*], Lan Huang [a], Yue Li [b], Quanzhong Shan [c], Datian Ye [d], Haiyan Ding [a], Jenchung Chien [e], Betau Hwang [e]

[a] *Department of Biomedical Engineering, School of Medicine, Room C217, Building of Medical Science, Tsinghua University, Beijing 100084, China*
[b] *Hefei Anheng Optic-electronic Co. Ltd., Hefei 230031, China*
[c] *Department of Clinical Laboratories, First Hospital of Tsinghua University, Beijing 100016, China*
[d] *Graduate School at Shenzhen, Tsinghua University, Shenzhen 518055, China*
[e] *Department of Pediatrics, Taipei Veterans General Hospital, Taipei, China*

Received 15 January 2008; received in revised form 22 January 2008; accepted 23 January 2008

Abstract

In this paper, the biological tissue oxygen saturation (rSO_2) is obtained non-invasively and in real time based on near infrared spectroscopy (NIRS) using two emitting wavelengths and two detectors, where the tissue is covered with overlying tissues. Our group developed an NIRS oximeter based on the above principle independently, and validated it using liquid tissue model calibrations and animal experiments. The results indicate that (1) in the normal range of tissue oxygen saturation (40–70%), the rSO_2 measured by NIRS is accurate enough and little influenced by the background absorptions (such as the absorption of water) and overlying tissues (such as fat); (2) during cerebral hypoxia and recovery of three piglets, there is excellent correlation ($p < 0.001$) between cerebral rSO_2 and jugular venous oxygen saturation (SjO_2), meaning that the rSO_2 can be indicated by the SjO_2 to a large extent; during the death of the three piglets induced by heart beat stopping, cerebral rSO_2 decreases continuously to significantly low levels (<25%) because cerebral blood supply does not exist any more. All the above results are of explicit physiological importance.

Keywords: Tissue oxygen saturation; Jugular venous oxygen saturation; Overlying tissues; Non-invasive measurement

1. Introduction

In clinic it is significantly important to assess tissue oxygenation accurately in real time and to maintain it in the normal range accordingly. In biological tissue, oxygen combines mainly with deoxygenated hemoglobin (Hb) into oxygenated hemoglobin (HbO_2). Tissue oxygenation parameters include (1) the concentrations of Hb and HbO_2 in the tissue, C_{Hb} and C_{HbO_2}, which are the amount of Hb and HbO_2 in the unit volume of the tissue, respectively; and also the total concentration of hemoglobin, $C_{tHb} = C_{HbO_2} + C_{Hb}$; (2) the regional tissue oxygen saturation, rSO_2, is defined as

$$rSO_2 = \frac{C_{HbO_2}}{C_{HbO_2} + C_{Hb}} \times 100\% = \frac{C_{HbO_2}}{C_{tHb}} \times 100\% \quad (1)$$

Among the above tissue oxygenation parameters, rSO_2 is mostly concerned in clinic. In biological tissue, there are a large amount of arterioles, venules and capillaries. The rSO_2 is actually the weighted average of the oxygen saturation in the above microvessels. Because the blood in the venules flows relatively slowly, its oxygen saturation is dominant in the rSO_2. For example, 60–80% of the blood

* Corresponding author. Tel.: +86 10 62773223 82.
E-mail address: dhs-dea@tsinghua.edu.cn (H. Ding).

1002-0071/$ - see front matter
doi:10.1016/j.pnsc.2008.01.035

in the brain cortex is from the venules, 15–20% is from the arterioles, and the other is from the capillaries [1].

Nowadays there are mainly two indirect methods for assessing tissue oxygenation especially tissue rSO_2. One is invasive blood gas analysis, which extracts the blood from large vessels and measures its oxygen saturation to assess tissue rSO_2. Even though blood gas analysis is a "golden criteria" in measuring blood oxygen saturation, it is invasive because large vessels need to be intubated, and unavailable for continuous monitoring. Moreover, tissue rSO_2 is still different with the blood oxygen saturation from the large vessels. The other is monitoring the pulse oxygen saturation (SpO_2) at the finger tip non-invasively [2]. The principle of SpO_2 depends on the pulsation of the arterioles at the finger tip. Therefore, the SpO_2 is actually arterial blood oxygen saturation and essentially different with tissue rSO_2.

According to the above defects, it is clinically required to monitor tissue oxygenation non-invasively, continuously, directly and in real time. Near infrared spectroscopy (NIRS), whose basic principle is based on the absorption spectra of Hb and HbO_2 in the near infrared band of 700–900 nm [3], is such a method. Using the incident light with constant intensity, continuous-wave (CW) NIRS [4] is suitable for clinical monitoring because of its convenience. Now CW NIRS has been clinically applied in many areas by some groups [5–8].

There are still some defects in the CW NIRS nowadays. Firstly, only the concentration changes of tissue C_{Hb} and C_{HbO_2} comparing with their original values, while not the value of tissue rSO_2, are obtained generally. Secondly, the detected tissues (such as the brain cortex and skeletal muscle) are generally covered with the overlying tissues (such as the skin, skull, and fat), and the influences by the latter cannot be ignored in many cases. According to the above problems, we use CW NIRS under two wavelengths and two detectors to non-invasively obtain the rSO_2 of the tissue being covered with the overlying tissues. Our group developed a CW NIRS oximeter independently (TSAH-100). To validate the above CW NIRS for clinical applications, we measured the rSO_2 using the NIRS oximeter during liquid tissue model calibrations and animal experiments. The results indicate that the rSO_2 is accurate enough and little influenced by the background absorptions and overlying tissues. And that, during cerebral hypoxia and recovery of three piglets, there is excellent correlation between the cerebral rSO_2 measured by the NIRS oximeter and the jugular venous oxygen saturation (SjO_2) measured by blood gas analysis; during the death of the piglets induced by heart beat stopping, the cerebral rSO_2 decreases continuously to significantly low levels (all <25%). All the above results are of explicit physiological importance.

2. Basic principles of tissue rSO_2

In the near infrared band of 700–900 nm, biological tissue is strongly scattering. If a beam of near infrared light is incident into biological tissue, the average propagation trace of large amount of photons is curved and the partial pathlength (PPL) in the detected tissue (covered with the overlying tissues) is different from the distance (r) between the light source and the detector (Fig. 1). In this band, Hb and HbO_2 are the main absorbers in biological tissue and their absorption spectra are significantly different [3]. Using the incident light with constant intensity, the light attenuation by the tissue can be described by the modified Lambert–Beer law [4]

$$OD = \log(I_0/I) = (\varepsilon_{HbO_2} C_{HbO_2} + \varepsilon_{Hb} C_{Hb}) \cdot r \cdot \mathrm{DPF} + G \quad (2)$$

Here, I_0 and I are the light intensity of the incident and emitted light; OD is the optical density and describes the light attenuation; ε's are the extinction coefficients, which are dependent on the absorbers and the wavelengths [3]; DPF is named as the differential pathlength factor, which is equal to PPL/r and is generally independent on the wavelengths in the near infrared band [9]; and G is the unknown background attenuation, which is the attenuation by the background substances (mainly water) besides Hb and HbO_2.

To eliminate the influences of G in Eq. (2), we use two detectors and ensure that the distance between each one and the light source (r_1 and r_2 for the nearer and the farther detector, respectively) is large enough that the emitted light received by each one may propagate across the detected tissue (Fig. 2). If the distance between the two detectors is not very large (approximately 10 mm would be OK), it can be considered that the G's corresponding to the two detectors under the same wavelength are approximately equal, and the DPF is independent on the distance. Subtracting Eq. (2) under r_1 and r_2, we can obtain

$$\sigma OD = OD_2 - OD_1 = (\varepsilon_{HbO_2} C_{HbO_2} + \varepsilon_{Hb} C_{Hb}) \cdot \mathrm{DPF} \cdot (r_2 - r_1) \quad (3)$$

Here, the subscripts 1 and 2 correspond to the two detectors. The σOD can be optically detected. Because there are two unknown parameters (C_{Hb} and C_{HbO_2}), two wavelengths (λ_1 and λ_2) need to be used, and the rSO_2 can be obtained by substituting Eq. (1) to Eq. (3)

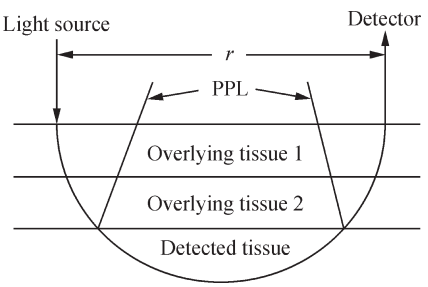

Fig. 1. The average propagation trace of large amount of photons, where the PPL and r are marked. When the detected tissue is the skeletal muscle, the overlying tissues 1 and 2 are the skin and the fat, respectively. When the detected tissue is the brain cortex, the overlying tissues 1 and 2 are the scalp and the skull, respectively.

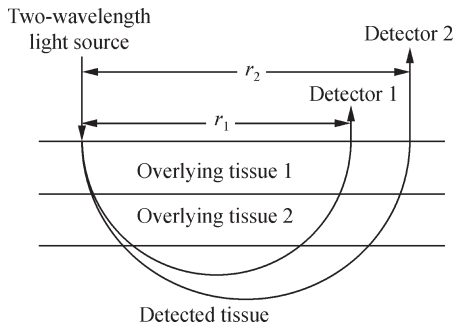

Fig. 2. The outline of measuring tissue rSO_2 using two wavelengths and two detectors.

$$rSO_2 = \frac{\varepsilon_{Hb}^{\lambda_1} - \varepsilon_{Hb}^{\lambda_2} \frac{\sigma OD^{\lambda_1}}{\sigma OD^{\lambda_2}}}{\frac{\sigma OD^{\lambda_1}}{\sigma OD^{\lambda_2}} (\varepsilon_{HbO_2}^{\lambda_2} - \varepsilon_{Hb}^{\lambda_2}) - (\varepsilon_{HbO_2}^{\lambda_1} - \varepsilon_{Hb}^{\lambda_1})} \quad (4)$$

3. Instrumentation

The non-invasive CW NIRS tissue oximeter (TSAH-100, Fig. 3) developed by our group was used, and tissue rSO_2 was detected based on the above principles. The probe of TSAH-100 consisted of a two-wavelength light source (760 nm and 850 nm) and two detectors.

4. Experimental protocol

4.1. Liquid tissue model calibrations

We calibrated the NIRS oximeter (TSAH-100) using the blood gas analyzer (Nova m7, Nova Co. US). The oxygen saturation of the *in vitro* liquid tissue model was measured by the above two instruments simultaneously, in order to assess the influences of the background absorptions and the overlying tissues. The oxygen saturations of the model detected by the oximeter and the analyzer were denoted by S and S_0, respectively, where S_0 was considered to be the accurate value. The total volume of the model was 1000 ml, including 40 ml human whole blood (its volume ratio is 4%), 25 ml scattering media (intralipid-20%) and 935 ml buffer solution, so that the optical characteristics of the model was close to biological tissues in the near infrared band. On the probe, the distances between the light source and the two detectors were 30 mm and 40 mm, respectively.

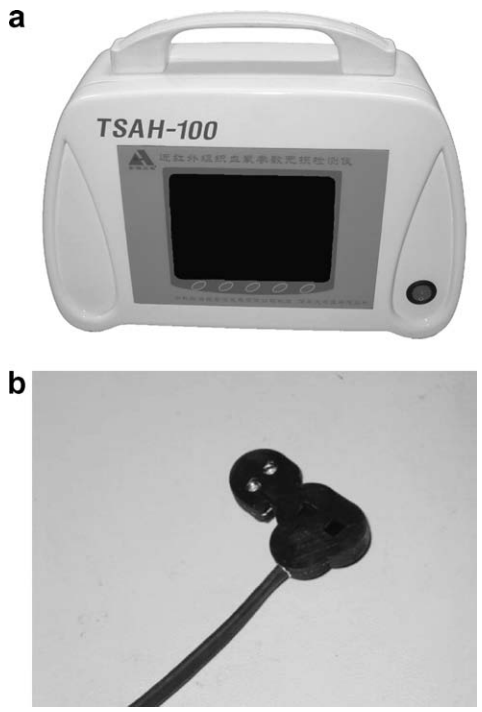

Fig. 3. (a) The non-invasive CW NIRS tissue oximeter (TSAH-100); (b) the probe.

4.1.1. Without the overlying tissue

Firstly, the model was sufficiently oxygenated by inflating pure oxygen into it for 5 min at 300 ml/min. Then the oximeter was turned on after its probe was tightly fixed onto the liquid surface. To decrease the oxygen saturation of the model, we used sodium hydrosulfite ($Na_2S_2O_4$) as the reducer, which was soluble in the model. Every time $Na_2S_2O_4$ of about 10 mg was added into the model by stirring at the same time, the oxygen saturation of the model decreased rapidly for about 10 percentage points and then could be stable at this lower level for about 30 min. Therefore, multiple steady oxygenation levels decreasing stepwise could be obtained. On each oxygenation level, S_0 was measured using blood gas analysis, and S was measured using the NIRS oximeter simultaneously. Repeating this procedure until S_0 was close to 0%, the calibration line ($S = kS_0 + b$) could be obtained by linear regression, where k, b and the correlation coefficient (R) could all be calculated.

4.1.2. With the overlying tissue

We covered a 5 mm-thick piece of pig fat onto the model surface, and then fixed the NIRS probe tightly onto the upper surface of the fat. Repeating the procedures in the above section, the calibration results with the overlying tissue could also be obtained, including $S = kS_0 + b$ and R.

4.2. Animal experiments

The animal experiments were cooperatively carried out by our group, Taipei Veterans General Hospital, and Taipei Yang Ming University, in the operation room of Taipei Veterans General Hospital. Three piglets (9, 10, and 12 days after birth, weighted 2.2, 2.4, 2.0 kg, respectively) were studied. Anesthesia was firstly induced by intravascular injection of ketamine (33 mg/kg). By trachea incision and intubation, pure oxygen was inhaled at 40/min by the ventilator (Harvard Rodent Ventilator Model 683). Cerebral rSO_2 of each piglet was monitored using our NIRS oximeter non-invasively in real time, where the probe was fixed onto the forehead. The blood pressure, the heart rate and the SpO_2 of each piglet were detected using the multiparameter monitor (Aligent Co.) simultaneously. The environmental temperature was 25 °C constantly.

For each piglet after the rSO_2 was stable for 4–6 min, cerebral hypoxia was induced by changing the oxygen ratio of the inhaling air into 21% and decreasing the respiration rate for 5/min stepwise using the ventilator. The time duration of each step was 5 min. When the heart rate was lower than 60/min, cerebral oxygenation was recovered by inhaling pure oxygen and resuming the respiration rate to 40/min again. During the whole procedure including the above hypoxia and recovery, cerebral rSO_2 was non-invasively recorded every 5 min, and the jugular venous oxygen saturation (SjO_2) was invasively detected also every 5 min simultaneously using the blood gas analyzer (GASTAT-3). Then the correlation between the rSO_2 and the SjO_2 was calculated and statistically discussed [10]. After the recovery of cerebral oxygenation, each piglet was sacrificed by injecting 10% KCl for 5 ml. During this stage, the heart beat stopped, and the rSO_2 was monitored in real time and recorded every minute.

All the animal experiments were approved by the Experiment Animal Care and Use Committee of Taipei Veterans General Hospital.

5. Results

5.1. Liquid tissue model calibrations

Three times of the calibration results between S and S_0 as well as their average result without the overlying tissue (the 5 mm-thick fat), and all those results with the overlying tissue, are shown in Table 1. Therefore, under each condition (without or with the overlying tissue), each of the three calibration lines is very close to the corresponding average.

Fig. 4 shows the ideal calibration line, which is $S = S_0$, and the average calibration lines without and with the overlying tissue. When S_0 was in the range of 40–70%, the above three lines are very close to each other. Only when S_0 is close to 0% or 100%, there is a certain error among them, which is more obvious with the overlying tissue.

5.2. Animal experiments

5.2.1. Cerebral rSO_2 vs. jugular SjO_2

During cerebral hypoxia of the three piglets induced by decreasing the respiration rate stepwise, both cerebral rSO_2 and jugular SjO_2 decrease significantly. At the beginning moment of the recovery of cerebral oxygenation (the hypoxia has been kept for 30–40 min), both the rSO_2 and the SjO_2 are lower than 30%. After this moment, because of inhaling pure oxygen, both of them increase significantly. During the whole procedure including the above hypoxia and recovery, there is excellent statistical correlation between the rSO_2 and the SjO_2 for each piglet ($R = 0.900$, 0.896, and 0.853, respectively, and $p < 0.001$ for each one, see Fig. 5).

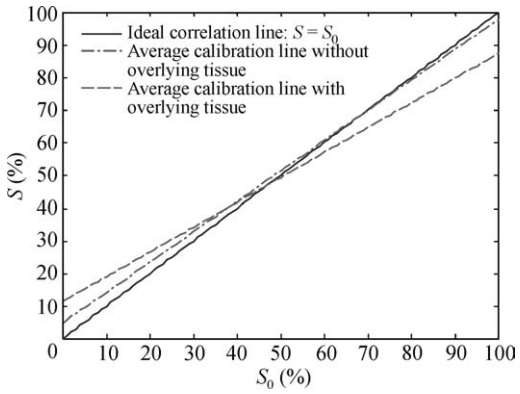

Fig. 4. The ideal calibration line ($S = S_0$) and the average calibration lines without and with the overlying tissue.

5.2.2. Cerebral rSO_2 during death

For each piglet, during the death induced by the heart beat stopping after KCl injection, its cerebral rSO_2 decreases significantly and is less than 25% finally (Fig. 6). The SpO_2 cannot be detected during death.

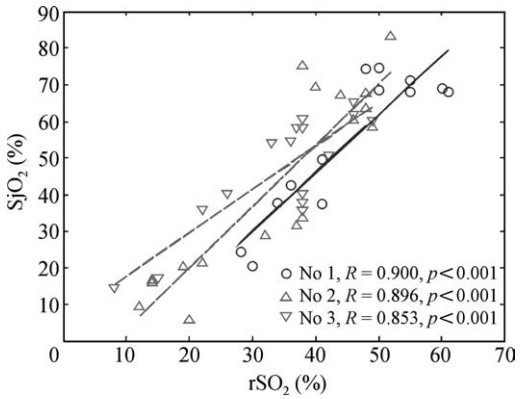

Fig. 5. The rSO_2 and the SjO_2 of the three piglets during the whole procedure including the hypoxia and recovery.

Table 1
The calibration results

No.	Without the overlying tissue			With the overlying tissue		
	k	b	R	k	b	R
1	0.91	3.70	0.998	0.73	11.18	0.998
2	0.93	5.43	0.991	0.74	10.47	0.985
3	0.95	5.35	0.970	0.81	12.45	0.994
Average (mean ± SD)	0.93 ± 0.02	4.83 ± 0.98		0.76 ± 0.05	11.37 ± 1.01	

6. Discussion and conclusion

Tissue rSO_2 is of great clinical importance and can be monitored non-invasively, continuously and in real time using CW NIRS with two wavelengths and two detectors. Generally, the detected tissue is covered with overlying tissues. If the distances between the light source and the detectors are too small, the average penetration depth of a large amount of photons is also too small to penetrate the detected tissue. Therefore, the rSO_2 of the detected tissue cannot be derived from the detected light. On the contrary, if the above distances are too large, the detected light is attenuated too much because the average propagation pathlength in the tissue (including the detected and the overlying tissues) is too long. Therefore, there may be obvious errors in the rSO_2 because the detected light is too weak. To obtain the rSO_2 of the detected tissue accurately against the influences by the overlying tissues, the above distances must be rationally selected so that the optimal coupling between the probe and the detected tissue may be achieved. In our previous research on detecting the oxygenation of the skeletal muscle (the skin and the fat are the overlying tissues), we discussed the optimal distances under different thicknesses of the overlying tissues using Monte-Carlo simulation [11] and ergometer experiments [12]. Similarly, we also discussed the optimal distances on detecting cerebral oxygenation (the scalp and the skull are the overlying tissues). The results indicate that the optimal distances between the light source and the two detectors are 30 mm and 40 mm during detecting adult cerebral rSO_2, while the optimal distances are 20 mm and 30 mm during detecting neonatal cerebral rSO_2.

For clinical applications of the NIRS and the oximeter (TSAH-100), liquid tissue model calibrations and animal experiments are made for validation.

6.1. Liquid tissue model calibrations: accessing the accuracy of rSO_2

6.1.1. Without the overlying tissue

From Table 1, the average calibration line is $S = 0.93S_0 + 4.83$. The continuous line depicted in Fig. 7 shows the error between it and the ideal calibration line ($S = S_0$) when S_0 is 0–100%. Thus, the error exists mainly when S_0 is close to 100% or 0%, which is caused by the background absorptions. Here, we define μ_w as the background absorption coefficient, which is generally independent on wavelength in the near infrared band [13] and much lower than the absorption coefficients of Hb and HbO_2. Then the background attenuation G in Eq. (2) can be described as $G = \mu_w \cdot r \cdot \mathrm{DPF}$, and so

$$OD = (\varepsilon_{\mathrm{HbO_2}} C_{\mathrm{HbO_2}} + \varepsilon_{\mathrm{Hb}} C_{\mathrm{Hb}}) \cdot r \cdot \mathrm{DPF} + \mu_w \cdot r \cdot \mathrm{DPF} \quad (5)$$

Subtracting Eq. (5) under r_1 and r_2 and from Eq. (1), the accurate value of oxygen saturation (also denoted by S_0) can be obtained

$$\begin{aligned} S_0 &= \frac{\varepsilon_{\mathrm{Hb}}^{\lambda_1} - \varepsilon_{\mathrm{Hb}}^{\lambda_2} \frac{\sigma OD^{\lambda_1}}{\sigma OD^{\lambda_2}}}{\frac{\sigma OD^{\lambda_1}}{\sigma OD^{\lambda_2}} (\varepsilon_{\mathrm{HbO_2}}^{\lambda_2} - \varepsilon_{\mathrm{Hb}}^{\lambda_2}) - (\varepsilon_{\mathrm{HbO_2}}^{\lambda_1} - \varepsilon_{\mathrm{Hb}}^{\lambda_1})} \\ &\quad + \frac{\frac{\mu_w}{C_{\mathrm{tHb}}} \left(1 - \frac{\sigma OD^{\lambda_1}}{\sigma OD^{\lambda_2}}\right)}{\frac{\sigma OD^{\lambda_1}}{\sigma OD^{\lambda_2}} (\varepsilon_{\mathrm{HbO_2}}^{\lambda_2} - \varepsilon_{\mathrm{Hb}}^{\lambda_2}) - (\varepsilon_{\mathrm{HbO_2}}^{\lambda_1} - \varepsilon_{\mathrm{Hb}}^{\lambda_1})} \\ &= S + \frac{\frac{\mu_w}{C_{\mathrm{tHb}}} \left(1 - \frac{\sigma OD^{\lambda_1}}{\sigma OD^{\lambda_2}}\right)}{\frac{\sigma OD^{\lambda_1}}{\sigma OD^{\lambda_2}} (\varepsilon_{\mathrm{HbO_2}}^{\lambda_2} - \varepsilon_{\mathrm{Hb}}^{\lambda_2}) - (\varepsilon_{\mathrm{HbO_2}}^{\lambda_1} - \varepsilon_{\mathrm{Hb}}^{\lambda_1})} \end{aligned} \quad (6)$$

Here, S is the rSO_2 derived from Eq. (4), where the influences of the background absorptions are not considered. Then the error E between S and S_0 can be derived

$$E = S - S_0 = \frac{\frac{\mu_w}{C_{\mathrm{tHb}}} \left(\frac{\sigma OD^{\lambda_1}}{\sigma OD^{\lambda_2}} - 1\right)}{\frac{\sigma OD^{\lambda_1}}{\sigma OD^{\lambda_2}} \left(\varepsilon_{\mathrm{HbO_2}}^{\lambda_2} - \varepsilon_{\mathrm{Hb}}^{\lambda_2}\right) - (\varepsilon_{\mathrm{HbO_2}}^{\lambda_1} - \varepsilon_{\mathrm{Hb}}^{\lambda_1})} \quad (7)$$

It is difficult to obtain S_0 from Eq. (6), because μ_w is generally unknown. But in the liquid tissue model, the background attenuation is mainly caused by water. The μ_w of water in the near infrared band is about 0.01/cm [13]. The concentration of the total hemoglobin in human whole blood is generally about 150 g/l. Because the blood volume ratio of the liquid tissue model is 4% and the molecular weight of hemoglobin is about 64,500, it can be calculated that the C_{tHb} of the model is about 93 μmol/l. Therefore,

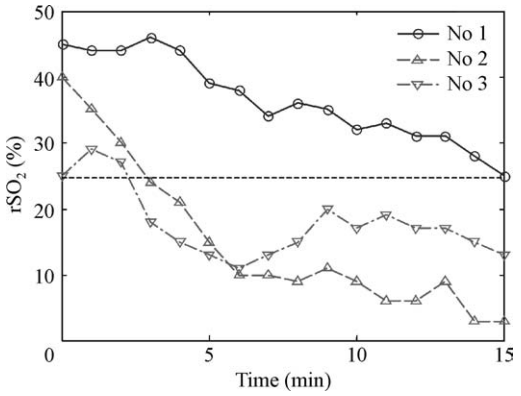

Fig. 6. Cerebral rSO_2 of the three piglets during death.

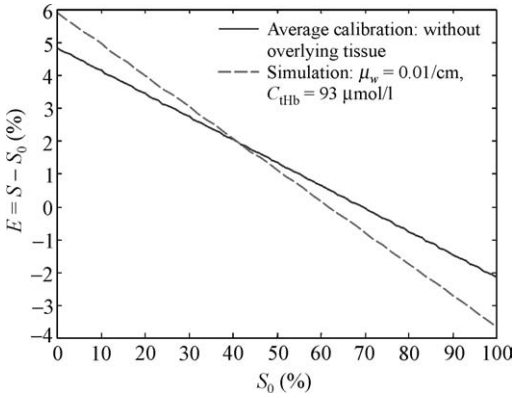

Fig. 7. The error between S and S_0 ($E = S - S_0$) obtained by the simulation using Eq. (7) and the calibrations.

when S_0 is in the range of 0–100%, the error E can be simulated from Eq. (7) (the dashed line shown in Fig. 7). Here, the two wavelengths are $\lambda_1 = 760$ nm and $\lambda_2 = 850$ nm.

The two lines shown in Fig. 7 are consistent (the difference between them is less than 2%). When S_0 is close to 0%, there is $S > S_0$; when S_0 is close to 100%, there is $S < S_0$. Therefore, when the changing range of the S_0 is 0–100%, the corresponding changing range of S is less than that of S_0 because of the background absorptions. However, when S_0 is in the range of 40–70% which includes the normal range of biological tissue rSO_2, the error E obtained by both the simulation (using Eq. (7)) and the calibrations is very small (in the range of ±2%). Therefore, the influences of the background absorptions can be ignored as detecting biological tissue rSO_2.

6.1.2. With the overlying tissue

Here, the distances between the light source and the two detectors are 30 mm and 40 mm, respectively, and the thickness of the overlying tissue is 5 mm. The results by Monte-Carlo simulations indicate that the optimal coupling between the probe and the detected liquid tissue model can be achieved, and the oxygen saturation of the model can be derived from the received light by the two detectors. Fig. 4 shows that the influence of the overlying tissue is also relatively obvious when S_0 is close to 100% or 0%, namely the changing range of S is also less than that of S_0. Note that here the error E between S and S_0 is more obvious than the condition without the overlying tissue. The reason is that E is induced not only by the overlying tissue but also by the background absorptions in the model. Similarly, when S_0 is in the range of 40–70% which includes the normal range of biological tissue rSO_2, E is also small. Therefore, the influences of the overlying tissues can also be ignored as detecting biological tissue rSO_2 when the optimal coupling between the probe and the detected tissue is achieved.

6.2. Animal experiments: Assessing the physiological meanings of rSO_2

For each piglet during the whole procedure including cerebral hypoxia and recovery, there is excellent correlation between cerebral rSO_2 and jugular SjO_2 ($p < 0.001$, Fig. 5). According to its definition, cerebral rSO_2 can be indicated by jugular SjO_2 to a large extent because the blood in the cerebral venules flows firstly into the jugular venous and then into the superior vena cava. Therefore, the rSO_2 measured by the NIRS oximeter is of explicit physiological importance. But the rSO_2 and the SjO_2 are not absolutely consistent, which may be caused by the following two aspects. Firstly, the venous blood that flows into the jugular is not only from the brain cortex but also from other parts on the head such as the face and the scalp. Therefore, the rSO_2 and the SjO_2 are not absolutely equal. Secondly, cerebral edema and ecchymoma may be induced by hypoxia. The oxygen saturation of the ecchymoma is generally very low, and its contribution to cerebral rSO_2 cannot be reflected by the SjO_2.

During the death of each piglet induced by the heart beat stopping, cerebral rSO_2 decreases significantly and continuously and is finally less than 25% (Fig. 6). The reason is that cerebral oxygen supply does not exist any more induced by the stopping of the arterial blood flow. At the same time, the SpO_2 cannot be detected because its principle depends on the pulsation of the arterioles at the finger tip and that pulsation is very weak during death. This also indicates the explicit physiological meanings of the rSO_2 and its advantages comparing with the SpO_2. In summary, according to the results of the animal experiments, the CW NIRS as well as the TSAH-100 oximeter is accurate enough for clinical applications.

Acknowledgements

This work was supported by National Natural Science Foundation of China (Grant Nos. 39670799, 69778024, and 60578004) and China Postdoctoral Science Foundation (Grant No. 20070410514). The authors thank Professor B. Chance from University of Pennsylvania, US, for his earnest helps.

References

[1] Mchedlishvili G. Arterial behavior and blood circulation in the brain. New York: Plenum Press; 1986, 42–95.
[2] Yitzhak M, Burt D. Noninvasive pulse oximetry utilizing skin reflectance photoplethysmography. IEEE Trans Biomed Eng 1988;35:798–805.
[3] Matcher SJ, Elwell CE, Cooper CE, et al. Performance comparison of several published tissue near-infrared spectroscopy algorithms. Anal Biochem 1995;227:54–68.
[4] Shiga T, Tanabe K, Nakase Y, et al. Development of a portable tissue oximeter using near infrared spectroscopy. Med & Biol Eng & Comp 1995;33:622–6.
[5] Watkin SL, Spencer SA, Dimmock PW, et al. A comparison of pulse oximetry and near infrared spectroscopy (NIRS) in the detection of hypoxemia occurring with pauses in nasal airflow in neonates. J Clin Monit 1999;15:441–7.
[6] Kunihara T, Sasaki S, Shiiya N, et al. Near infrared spectrophotometry reflects cerebral metabolism during hypothermic circulatory arrest in adults. Asaio J 2001;47:417–21.
[7] Boas DA, Gaudette T, Strangman G, et al. The accuracy of near infrared spectroscopy and imaging during focal changes in cerebral hemodynamics. Neuroimage 2001;13:76–90.
[8] Ding H, Wang G, Lei W, et al. Non-invasive quantitative assessment of oxidative metabolism in quadriceps muscles by near infrared spectroscopy. Br J Sports Med 2001;35:441–4.
[9] Hiraoka M, Firbank M, Essenpreis M, et al. Monte Carlo simulation of light transport through inhomogeneous tissue. Proc SPIE 1993;1888:149–59.
[10] Feinstein AR. Principles of medical statistics. Boca Raton: CHAPMAN & HALL/CRC Press; 2002, 379.
[11] Wang L, Jacques SL, Zheng L. MCML-Monte Carlo modeling of light transport in multi-layered tissues. Comput Meth Programs Biomed 1995;47:131–46.
[12] Wang F, Ding H, Tian F, et al. Influence of overlying tissue and probe geometry on the sensitivity of a near-infrared tissue oximeter. Physiol Meas 2001;22:201–8.
[13] Chance B, Cope M, Gratton E, et al. Phase measurement of light absorption and scatter in human tissue. Rev Sci Instrum 1998;69:3457–81.